magnetochemistry

MDPI

Article

Magnetic, Electric and Optical Properties of Ion Doped $CuCr_2O_4$ Nanoparticles

Angel Todorov Apostolov [1], Iliana Naumova Apostolova [2] and Jilia Mihailowa Wesselinova [3,*]

[1] Civil Engineering and Geodesy, Faculty of Hydrotechnics, University of Architecture, Hristo Smirnenski Blvd. 1, 1046 Sofia, Bulgaria
[2] Department of Physics, University of Forestry, Kl. Ohridsky Blvd. 10, 1756 Sofia, Bulgaria
[3] Department of Physics, University of Sofia, J. Bouchier Blvd. 5, 1164 Sofia, Bulgaria
* Correspondence: julia@phys.uni-sofia.bg

Abstract: The magnetic, electric and optical properties of pure and ion doped $CuCr_2O_4$ - bulk and nanoparticles are investigated theoretically. The magnetization M_s and the band gap E_g decrease with increasing particle size. By Co ion doping M_s and the polarization P show a maximum whereas by Pr ion doping they decrease with increasing the doping concentration. The dielectric constant decreases with enhancing Pr dopants. It is shown that the difference between the doping and host ions radii leads to appearing of a compressive or tensile strain and to different exchange interaction constants in the doped state. E_g decreases by Co doping, whereas it increases by Pr doping.

Keywords: $CuCr_2O_4$ nanoparticles; ion doping; magnetization; polarization; band gap energy

check for updates

Citation: Apostolov, A.T.; Apostolova, I.N.; Wesselinowa, J.M. Magnetic, Electric and Optical Properties of Ion Doped $CuCr_2O_4$ Nanoparticles. *Magnetochemistry* **2022**, *8*, 122. https://doi.org/10.3390/magnetochemistry8100122

Academic Editors: Kamil Gareev and Ksenia Chichay

Received: 9 September 2022
Accepted: 3 October 2022
Published: 7 October 2022

1. Introduction

Spinel structured chromium oxides ACr_2O_4 (A = Cu, Mn, Fe, Co, and Ni) exhibit a wide range of electronic, magnetic, and optical properties [1]. Their physical properties depend upon the distribution of cations among the tetrahedral (A) and octahedral sites (B), and relative superexchange interactions via anions. They have a great research interest in the last years due to their multiferroic (MF) properties and applications in nanoscience and nanotechnology. Moreover, $CuCr_2O_4$ (CCO) structure has attracted also large attention due to thermal and chemical stability and various applications such as: photocatalytic degradation, photocatalytic H_2 production, oxidation of carbon monoxide, and water treatment [2]. CCO is a normal spinel in which Cr^{3+} and Cu^{2+} ions are situated at the octahedral (B) and tetrahedral (A) sites, respectively [3]. The strongly negative J_{BB} (Cr-O-Cr) and J_{AB} (Cu-O-Cr) exchange interactions play an important role in controlling the magnetic properties of chromites and observing a ferrimagnetic phase. The magnetization data of the bulk CCO compounds indicate ferrimagnetic order below T_C^{FM} = 122 K [3]. Enhanced magnetism and Curie temperature are observed in CCO thin films due to substrate effects [4,5]. Ali et al. [6] presented a detailed study of magnetic and magnetocaloric effect of the 3d-metal chromites ACr_2O_4 (where A = Mn, Fe, Co, Ni, Cu, and Zn) near T_C and T_N. Enhanced magnetism and Curie temperature are observed in CCO thin films due to substrate effects [4,5]. Ye et al. [7] studied different properties of CCO single crystals. The effects of Co doping on the MF order in CCO is reported recently by Chatterjee et al. [8]. Structure and vibrational studies of La doped CCO are performed recently by Rajeswari et al. [9]. Jahn-Teller and geometric frustration effects on the structural and magnetic ground states of substituted spinels (Ni,A)Cr_2O_4, (A = Mn/Cu) are studied by Yadav et al. [10]. Multiferroicity is found in other chromites, too, for example $FeCr_2O_4$ and $CoCr_2O_4$ spinels [11].

The optical spectra of CCO nanoparticles (NPs) are reported by Habibi et al. [12], Beshkar et al. [13], Krause et al. [14], Lahmar et al. [15]. The band gap E_g of CCO NPs (∼3.35 eV) as direct semiconductor [13] shows an increasing compared with that of the

bulk compound (around 1.2–1.4 eV) [15–17]. The band gap energy in Mn doped CCO NPs is studied in [18].

As mentioned above the effects of ion doping on the MF and optical properties of CCO are not so intensive studied - experimentally and theoretically. In the present paper we will investigate and explain for the first time using a microscopic model and the Green's function theory the appearance of MF and optical properties in pure and ion doped CCO NPs which can find different applications.

2. The Model

The s-d Hamiltonian which describes the CCO NP can be written as (for review see Refs. [19,20]:

$$H_{s-d} = H_{sp} + H_{el} + H_{sp-el}. \tag{1}$$

The Heisenberg Hamiltonian is corresponding for the ferrimagnetic properties of CCO:

$$H_{sp} = -\frac{1}{2}\sum_{i,j} J_{ij}\mathbf{S}_i \cdot \mathbf{S}_j - \sum_i D_i (S_i^z)^2, \tag{2}$$

where $\mathbf{S_i}$ is the Heisenberg spin operator. The Cu-Cu, Cr-Cr and Cu-Cr exchange interactions are antiferromagnetically ($J < 0$). D is single-ion anisotropy constant, $\mid D \mid << \mid J \mid$. By doping with Co or Pr ions the Hamiltonian is modified as follows, there appear some additive terms with $\propto (1-x)J(Cu-Cu)$ and $\propto xJ(Co-Co)$ or $\propto (1-x)J(Cr-Cr)$ and $\propto xJ(Pr-Pr)$, respectively.

H_{el} is the Hamiltonian of the conduction band electrons

$$H_{el} = \sum_{ij\sigma} t_{ij} c_{i\sigma}^{+} c_{j\sigma} + \frac{1}{2}\sum_{ijkl,\sigma\sigma'} v(ijkl) c_{i\sigma}^{+} c_{j\sigma'}^{+} c_{k\sigma'} c_{l\sigma}, \tag{3}$$

t_{ij} is the hopping integral, v is the Coulomb interaction and $c_{i\sigma}^{+}$ and $c_{i\sigma}$ are Fermi-creation and -annihilation operators.

The operator H_{sp-el} couples the spin and electron subsystems by an intra-atomic exchange interaction I_i:

$$H_{sp-el} = \sum_i I_i \mathbf{S}_i \mathbf{s}_i. \tag{4}$$

The spin operators s_i of the conduction electrons at site i can be expressed as $s_i^{+} = c_{i+}^{+} c_{i-}$, $s_i^z = (c_{i+}^{+} c_{i+} - c_{i-}^{+} c_{i-})/2$.

H_{sp-ph} describes the spin-phonon interactions which are important in CCO [21] and must be taken into account:

$$H_{sp-ph} = -\frac{1}{2}\sum_{i,j} F(i,j) Q_i S_j^z - \frac{1}{4}\sum_{i,j,r} R(i,j,r) Q_i Q_j S_r^z + h.c. \tag{5}$$

The normal coordinate Q_i can be expressed in terms of phonon creation a^{+} and annihilation a operators $Q_i = (2\omega_{0i})^{-1/2}(a_i + a_i^{+})$. F and R are the spin-phonon coupling constants in first and second order, respectively. h.c. represents the hermitian conjugate.

The total magnetization is $M = (M^A + M^B)$. The localized-spin magnetization $M^{A,B}$ for a given sublattice A or B and arbitrary spin S is calculated to

$$M^{A,B} = \frac{1}{N^2}\sum_{i,j}\left[(S^{A,B}+0.5)\coth[(S^{A,B}+0.5)\beta E_{ij}^{A,B}] - 0.5\coth(0.5\beta E_{ij}^{A,B})\right]. \tag{6}$$

$\beta = 1/k_B T$, $E_{ij}^{A,B}$ is the spin-wave excitation energy observed from the poles of the Green's functions $G_{ij}^{A,B} = \langle\langle S_i^{-A,B}; S_j^{+A,B}\rangle\rangle$.

For the approximate calculation of the Green's function G_{ij} we use a method proposed by Tserkovnikov [22]. After a formal integration of the equation of motion for G_{ij}, one obtains

$$G_{ij}(t) = -i\theta(t)\langle[S_i^-; S_j^+]\rangle \exp(-i\omega_{ij}(t)t) \tag{7}$$

where

$$\begin{aligned}\omega_{ij}(t) = \omega_{ij} \quad - \quad & \frac{i}{t}\int_0^t dt' t' \left(\frac{\langle[j_i(t); j_j^+(t')]\rangle}{\langle[S_i^-(t); S_j^+(t')]\rangle} \right. \\ - \quad & \left. \frac{\langle[j_i(t); S_j^+(t')]\rangle\langle[S_i^-(t); j_j^+(t')]\rangle}{\langle[S_i^-(t); S_j^+(t')]\rangle^2} \right)\end{aligned} \tag{8}$$

with the notation $j_i(t) = \langle[S_i^-, H_{interaction}]\rangle$. The time-independent term

$$\omega_{ij} = \frac{\langle[[S_i^-, H]; S_j^+]\rangle}{\langle[S_i^-; S_j^+]\rangle} \tag{9}$$

is the spin excitation energy in the generalized Hartree-Fock approximation. The time-dependent term in Equation (8) includes damping effects.

The spin induced electric polarization P_{ij} produced between the two magnetic moments S_i and S_j is given by [23]

$$P = ae_{ij} \times (S_i \times S_j), \tag{10}$$

where e_{ij} being the unit vector connecting the sites i and j, a is a proportional constant as determined by the spin exchange interaction and the spin-orbit interaction [24].

To obtain the dielectric function defined as [25]:

$$((\Lambda/(\epsilon(E)-1))_{\alpha\beta} + \Lambda\frac{k_\alpha k_\beta}{k^2})\tilde{G}^{\alpha\beta}(E) = \delta_{\alpha\gamma}; \qquad \Lambda = 4\pi Z^2/V, \tag{11}$$

where Z is the electron charge and V is the volume, we have calculated beyond the random phase approximation the longitudinal Green's function

$$\tilde{G}_{ij}^{zz}(E) = \frac{2(E^2 - (E_{fi})^2 + 2iE\gamma^{11})}{(E^2 - (E_{fi})^2 + 2iE\gamma^{11})(E + i\gamma^{33}) - E(\epsilon^{13})^2}. \tag{12}$$

E_{fi} and γ^{11} are the transverse pseudo-spin energy and its damping, whereas γ^{33} is the longitudinal damping. ϵ^{13} describes the coupling between the longitudinal and transverse modes. In order to determine ϵ' and ϵ'' we must evaluate the real and imaginary part of the Green's function (12).

Bulk CCO is a p-type semiconductor with a small band gap E_g of 1.4 eV [3]. E_g is defined by the difference between the valence and conduction bands [26]:

$$E_g = \omega^+(k=0) - \omega^-(k=k_\sigma) \tag{13}$$

with the electronic energies

$$\omega^\pm(k) = \epsilon_k - \frac{\sigma}{2}IM + \sum_{k'\sigma'}[v(o) - v(k-k')\delta_{\sigma\sigma'}]\langle n_{k'\sigma'}\rangle \tag{14}$$

observed from the Green's function $g(k,\sigma) = \ll c_{k,\sigma}; c_{k\sigma}^+ \gg$, $\sigma = \pm 1$. $\langle n_{k'\sigma'}\rangle$ is the occupation number distribution.

3. Numerical Results and Discussion

The following model parameters are used for the numerical calculations: J_1(Cu-Cu) = −0.26 meV, J_2(Cu−Cr) = −3.16 meV, J_3(Cr−Cr) = − 3.01 meV [27], D = −0.1 meV, I = 0.2 eV, T_N = 122 K, T_C = 170 K [8], F = 23 cm^{-1}, R = −18 cm^{-1}.

It should be noted that the magnetic exchange interactions are taken from Ref. [27]. The spin-phonon constants F and R are determined from the Raman spectra of CCO [28] at very low temperatures, taking two values at two different temperatures from the Raman phonon energy and solving the system of two equations with two unknown parameters (see for more [29]).

Let us emphasize that the exchange interaction $J_{ij} = J(r_i - r_j)$ depends on the distance between the spins, on the lattice parameters. It is different on the surface and the doped states, denoted as J_s and J_d, respectively, than in the bulk and undoped states, J_b. This is valid for all interaction constants. Moreover, the spin-phonon interaction renormalizes J to $J^{eff} = J + 2F^2/(\omega_0 - MR)$ which is now temperature dependent.

Firstly, the spontaneous magnetization M_s for a CCO NP is calculated in dependence on size at room temperature for the following relation $J_s > J_b$. It can be seen from Figure 1 that M_s increases with decreasing NP size. A similar behavior of M_s is observed by Iwata et al. [5]. This increase of M_s is due to surface and size effects, due to the changed number of next neighbors on the surface and the reduced symmetry. All these factors lead to the different exchange interaction constants on the surface and in the bulk. The properties are very sensitive to the surface value J_s of all interaction constants. With increasing J_s the increase of M_s with decreasing N is stronger, the value of M_s is larger (see Figure 1, curve 2.) Below a critical size of N_{cr} = 3 the ferrimagnetism disappears, we have superparamagnetism which is not studied here. The magnetic transition temperature T_N also decreases with increasing the NP size.

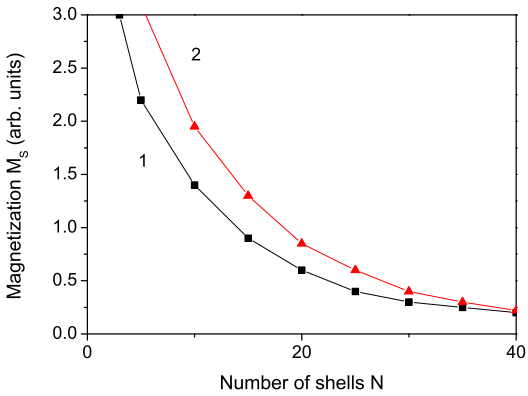

Figure 1. Dependence of the magnetization M_s on the size in CCO for T = 300 K, $J_{s1,2,3}$ = 1.2 $J_{b1,2,3}$ (1) and 1.3 $J_{b1,2,3}$ (2).

The magnetization could be changed by doping with different ions. Firstly, we will substitute Cu^{2+} ions with ferromagnetic transition metal Co^{2+} ions. Thus, we can compare our results with those of Ref. [8] and check our model. By doping with Co^{2+} ions (0.65 $\dot{A}$ [30]), which radius is smaller than that of the Cu^{2+} ion (0.73 $\dot{A}$ [31]), there appears a compressive strain. This means that the exchange interaction constant at the doped state J_{d1} is larger than that in the undoped one J_{b1}, i.e., $J_{d1} > J_{b1}$. All other interaction constants in the doped states are assumed to be nearly the same as in the undoped ones. Thus the magnetization M_s increases with increasing Co doping concentration up to x = 0.6. After $x > 0.6$, where appears a secondary phase we use the relation $J_{d1} < J_{b1}$ and the magnetization M_s (see Figure 2, curve 1) begins to decrease, in accordance with the experimental data of Chatterjee et al. [8]. T_N decreases with increasing the Co dopants. It must be mentioned that T_N of bulk CCO is 122 K, whereas of $CoCr_2O_4$ it is 93 K. A similar behavior we expect

to obtain also by doping with Ni or Mn ions at the Cu site due to the relation between the ionic radii of these ions.

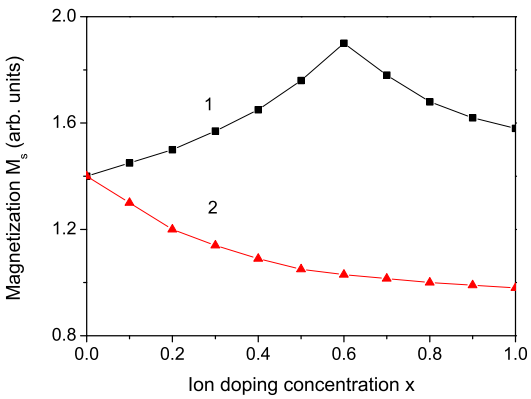

Figure 2. (Color online) Dependence of the magnetization M_s on the ion doping concentration x in CCO NP, N = 10, $J_{s1,2,3}$ = 1.2 $J_{b1,2,3}$ for (1) Co - for $0 \leq x \leq 0.6$ J_{d1} = 1.2 J_{b1} for $x > 0.6$ J_{d1} = 0.8 J_{b1}; (2) Pr - J_{d3} = 0.8 J_{b3}. All other interaction constants in the doped states are assumed to be nearly the same as in the undoped ones.

As the next we will consider the case of rare earth doping in a CCO NP. It is shown that for example by Pr^{3+} ion doping at the Cr^{3+} site, we observe a different behavior compared to the Co^{2+} doping at the Cu^{2+} site. We were looking for a doping with larger-sized ions, such as the rare earth ions which substitution is commonly used. Pr was randomly chosen, it could have been any other rare earth ion, La etc., which ionic radius is larger than that of Cr, and the results would have been qualitatively the same. Unfortunately, there are not experimental data for rare earth doped CCO. The lattice parameters increase with the substitution of the Pr ion, i.e., there appears a tensile strain. This is due firstly to the larger ionic radius of the Pr^{3+} ion (1.013 $\dot{A}$) in comparison with that of the Cr^{3+} ion (0.755 $\dot{A}$). The strain is also produced in the crystal's volume, due to this mismatch in ionic sizes. Moreover, the substitution of rare-earth ions into the copper-based spinel chromites creates a crystalline anisotropy. In addition, the system remains in stable form due to the balance of volume strain with crystalline anisotropy. Due to the tensile strain we have to use the following relation $J_{d3} < J_{b3}$. All other interaction constants in the doped states are assumed to be nearly the same as in the undoped ones. Then the spontaneous magnetization M_s decreases with increasing the Pr^{3+} doping concentration x (see Figure 2, curve 2). The substitution of the Pr^{3+} ions at the Cr^{3+} ion sites causes partial disorder and weakens the Cr^{3+}-O-Cr^{3+} super exchange interactions. Moreover, there appears changes of the valence of the Cr ion from Cr^{3+} with a high spin state to Cr^{2+} with a low spin state. This is due to the deviation from collinear to non-collinear order, leading to a decrease of T_N. This decrease in the magnetic phase transition temperature T_N may be also due to the fact that Pr-Cr interactions on the B sites are smaller than Cr-Cr interactions, $J(Pr - Cr) < J(Cr - Cr)$. Similar results for the spontaneous magnetization M_s and the magnetic phase transition temperature T_N we would obtain in the case of La ion doped CCO.

It is observed also the dependence of the polarization P on the ion doping concentration for Co and Pr doping ion substitution at Cu and Cr sites, respectively. The results are shown in Figure 3, curves 1 and 2, respectively. The discussion for the ion doping dependence of the polarization P is similar to that of the spontaneous magnetization $M_s(x)$. Moreover, the doping of Cu^{2+} with Co^{2+} systematically tunes the ferroelectric T_C as well as the magnetic ordering temperature T_N, which decrease with increasing x.

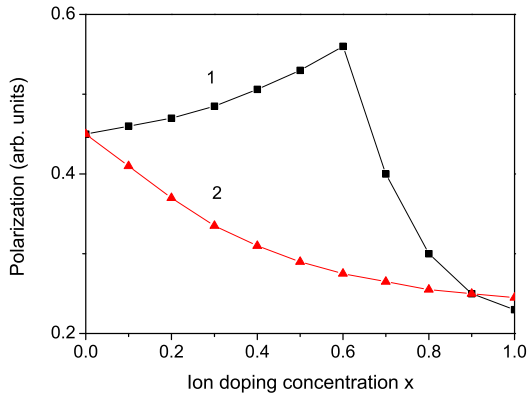

Figure 3. (Color online) Ion doping dependence of the polarization P in CCO NP, N = 10, $J_{s1,2,3}$ = 1.2 $J_{b1,2,3}$ for (1) Co - for $0 \leq x \leq 0.6$ J_{d1} = 1.2 J_{b1}, for $x > 0.6$ J_{d1} = 0.8 J_{b1}; (2) Pr - J_{d3} = 0.8 J_{b3}. All other interaction constants in the doped states are assumed to be nearly the same as in the undoped ones.

From Equations (11) and (12) the real ϵ' and imaginary ϵ'' part of the dielectric constant ϵ is calculated for small doping concentration x in Pr doped CCO NPs. The results are presented in Figure 4. It can be seen that both decrease with increasing x. The rare-earth ions substitute the ferric ions on the B-site due to their larger ionic radius which hinders the electrons exchange between the Cr^{2+} and Cr^{3+} ions. This leads to a decrease of the polarization P and the dielectric constant ϵ.

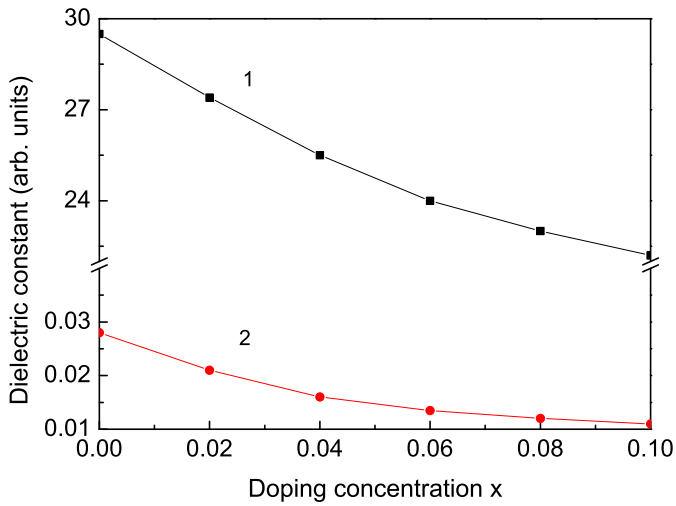

Figure 4. (Color online) The real (curve 1) and imaginary part (curve 2) of the dielectric constant ϵ as function of the Pr doping concentration in CCO NP, N = 10.

Finally, we will consider the band gap energy E_g of pure and ion doped CCO NPs. We observe that E_g increases strongly with decreasing NP size (see Figure 5), in agreement with the experimental results of Refs. [13,15]. By doping of a CCO NP with Co ions E_g decreases whereas by Pr ions it increases (see Figure 6). These results coincide with those of Lopez et al. [32]. The authors have studied the band gap energy in CdS thin films and have shown that the smaller the lattice parameter the larger the band gap. Band gap changes in doped semiconductors could be due as a result of exchange and Coulomb interactions. The band gap energy E_g increases with increasing the Coulomb interaction (not shown here). Unfortunately, there are not experimental data for E_g in ion doped CCO. Let us emphasize that the increase of the energy gap for semiconductors leads to decrease the absorption region and the substance may be transparent and the absorption edge shifted toward low wavelengths. This may be useful for solar cell applications.

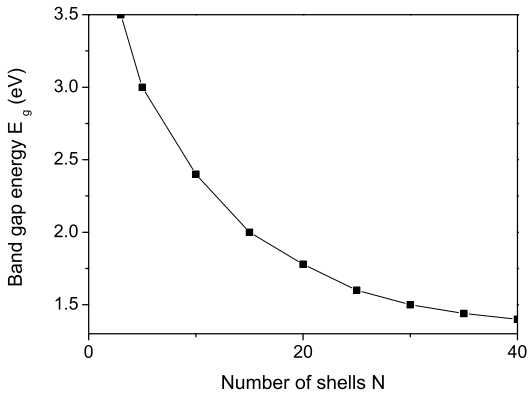

Figure 5. The band gap energy E_g in CCO as function of the size.

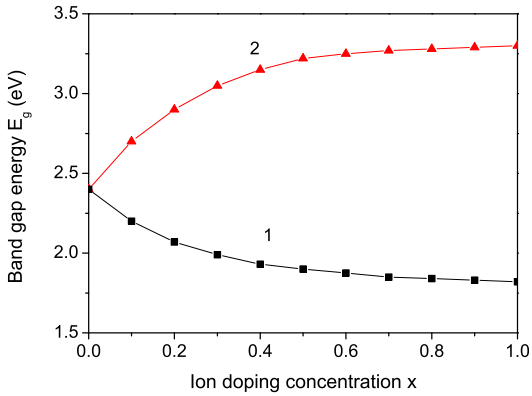

Figure 6. (Color online) Dependence of the band gap energy E_g on the ion doping concentration x in CCO NP, N = 10, $J_{s1,2,3}$ = 1.2 $J_{b1,2,3}$ for (1) Co - J_{d1} = 1.2 J_{b1}; (2) Pr - J_{d3} = 0.8 J_{b3}. All other interaction constants in the doped states are assumed to be nearly the same as in the undoped ones.

4. Conclusions

In the present paper we have investigated different properties of pure and ion doped CCO - bulk and NPs for the first time using a microscopic model. Our model is microscopic, because the exchange interaction constants are dependent on the lattice parameters, on the microstrain, on the crystal symmetry, on the number of nearest neighbors etc. They are renormalized through the spin-phonon interaction and are temperature dependent. So we can discuss the properties on microscopic level. They are connected with different strains which lead to different lattice parameters and different exchange interaction constants. Using the Green's function theory it is observed a decrease of the magnetization M_s and the band gap energy E_g with increasing NP size. The spontaneous magnetization M_s and the polarization P show a maximum value around x = 0.6 for Co dopants, whereas they decrease with increasing Pr doping concentration. The real and imaginary parts of the dielectric constant decrease with increasing Pr dopants. By the doping concentration of the band gap energy E_g it is vice versa. E_g decreases by Co doping and increases by Pr ion doping.

In summary, it is shown that in Co doped CCO NPs the MF properties, magnetization M and polarization P, as well as the coercivity are enhanced below x = 0.6, the phase transition temperatures T_N and T_C are reduced, so that this doping case is more appropriate for application in spintronics in comparison with the rare earth substitution, where M and P decrease with increasing Pr dopants. On the other hand, by Pr ion doping the band gap energy E_g is enhanced which can be used for solar cell applications.

It should be noted that the most observed properties of ion doped CCO NPs, for example the band gap energy, the dielectric constant, the rare earth ion doping, are not reported experimentally till now. Thus we hope that our results will be confirmed in the future.

Moreover, more experimental and fundamental theoretical investigations need to be done to find new materials with high multiferroic properties which can be applied in nanoscience and nanotechnology. We hope to have contributed to this view with this article.

Author Contributions: Conceptualization, J.M.W.; Data curation, A.T.A., I.N.A. and J.M.W.; Formal analysis, A.T.A., I.N.A. and J.M.W.; Funding acquisition, J.M.W.; Investigation, A.T.A. and I.N.A.; Methodology, I.N.A. and J.M.W. All authors contributed equally to this work. All authors have read and agreed to the published version of the manuscript.

Funding: This research received no external funding.

Institutional Review Board Statement: Not applicable.

Informed Consent Statement: Not applicable.

Data Availability Statement: The raw data that support the findings of this study are available from the corresponding author upon reasonable request.

Conflicts of Interest: The authors declare no conflict of interest.

References

1. Prasad, R.; Singh, P. Applications and Preparation Methods of Copper Chromite Catalysts: A Review. *Bull. Chem. React. Eng. Catal.* **2011**, *6*, 63–113. [CrossRef]
2. Kanti, P.K.; Chereches, E.I.; Minea, A.A.; Sharma, K.V. Experiments on thermal properties of ionic liquid enhanced with alumina nanoparticles for solar applications. *J. Therm. Anal. Calorim.* **2022**. [CrossRef]
3. Gurgel, T.T.; Buzinaro, M.A.; Moreno, N.O. Magnetization Study in $CuCr_2O_4$ Spinel Oxide. *J. Supercond. Nov. Magn.* **2013**, *26*, 2557–2559. [CrossRef]
4. Tripathi, T.S.; Yadav, C.S.; Karppinen, M. Transparent ferrimagnetic semiconducting $CuCr_2O_4$ thin films by atomic layer deposition. *APL Mater.* **2016**, *4*, 046106. [CrossRef]
5. Iwata, J.M.; Chopdekar, R.V.; Wong, F.; Nelson-Cheeseman, B.B.; Arenholz, E.; Suzuki, Y. Enhanced Magnetization of $CuCr_2O_4$ Thin Films by Substrate-Induced Strain. *J. Appl. Phys.* **2009**, *105*, 07A905. [CrossRef]
6. Ali, A.; Singh, Y. A magnetocaloric study on the series of 3d-metal chromites ACr_2O_4 where A = Mn, Fe, Co, Ni, Cu and Zn. *J. Magn. Magn. Mater.* **2020**, *499*, 166253. [CrossRef]
7. Ye, Z.-G.; Crottaz, O.; Vaudano, F.; Kubel, F.; Tissot, P.; Schmid, K. Single crystal growth, structure refinement, ferroelastic domains and phase transitions of the hausmannite $CuCr_2O_4$. *Ferroel.* **1994**. *162*, 103. [CrossRef]
8. Chatterjee, A.; Dey, J.K.; Majumdar, S.; Dippel, A.-C.; Gutowski, O.; Zimmermann, M.V.; Giri, S. Tuning of multiferroic order with Co doping in $CuCr_2O_4$: Interplay between structure and orbital order. *Phys. Rev. Mater.* **2019**, *3*, 104403. [CrossRef]
9. Rajeswari, G.; Prabavathi, N.; Tamizhdurai, P.; Prakasam, A.; Kumar, G. Enhancement of the structure, solar cells and vibrational studies of undoped $CuCr_{2O}4$ and La-doped $CuCr_2O_4$ semiconductor compounds. *Heliyon* **2022** *8*, e09233. [CrossRef] [PubMed]
10. Yadav, P.; Sharma, S.; Sau, T.; da Silva, I.; Lalla, N.P. Jahn-Teller and geometric frustration effects on the structural and magnetic ground states of substituted spinels (Ni,A)Cr_2O_4 (A = Mn/Cu). *J. All. Compd.* **2020**, *826*, 154139. [CrossRef]
11. Singh, K.; Maignana, A.; Simon, C.; Martin, C. $FeCr_2O_4$ and $CoCr_2O_4$ spinels: Multiferroicity in the collinear magnetic state? *Appl. Phys. Lett.* **2011**, *99*, 172903. [CrossRef]
12. Habibi, M.H.; Fakhri, F. Fabrication and Characterization of $CuCr_2O_4$ Nanocomposite by XRD, FESEM, FTIR, and DRS. *Synth. React. Inorg. Met.-Org. Nano-Met. Chem.* **2016**, *46*, 847. [CrossRef]
13. Beshkar, F.; Zinatloo-Ajabshir, S.; Salavati-Niasari, M. Preparation and characterization of the $CuCr_2O_4$ nanostructures via a new simple route. *J. Mater. Sci. Mater. Electron.* **2015**, *26*, 5043. [CrossRef]
14. Krause, M.; Sonnenberg, J.; Munnik, F.; Grenzer, J.; Huebner, R.; Garcia-Valenzuela, A.; Gemming, S. Formation, structure, and optical properties of copper chromite thin films for high-temperature solar absorbers. *Materialia* **2021**, *18*, 101156. [CrossRef]
15. Lahmar, H.; Kebir, M.; Nasrallah, N.; Trari, M. Photocatalytic reduction of Cr(VI) on the new hetero-system $CuCr_2O_4$/ZnO. *J. Mol. Catal. A Chem.* **2012**, *353–354*, 74–79. [CrossRef]
16. Ghorai, K.; Panda, A.; Hossain, A.; Bhattacharjee, M.; Chakraborty, M.; Bhattacharya, S.K.; Bera, P.; Kim, H.; Seikh, Md. M.; Gayen, A. Anatase TiO_2 decorated $CuCr_2O_4$ nanocomposite: A versatile photocatalyst under domestic LED light irradiation. *Appl. Surf. Sc.* **2021**. *568*, 150838. [CrossRef]
17. Benrighi, Y.; Nasrallah, N.; Chaabane, T.; Belkacemi, H.; Bourkeb, K.W.; Kenfoud, H.; Baaloudj, O. Characterization and application of the spinel $CuCr_2O_4$ synthesized by sol–gel method for sunset yellow photodegradation. *J. Sol.-Gel. Sc. Techn.* **2022**, *101*, 390. [CrossRef]

18. Soleimani, F.; Salehi, M.; Gholizadeh, A. Synthesis and characterization of new spinel $Mn_{0.5}Cu_{0.5}Cr_2O_4$ and degradation of Malachite Green from wastewater in comparison with $CuCr_2O_4$. *Int. J. Nano Dimens.* **2019**, *10*, 260–271.
19. Nagaev, E.L. Spin Polaron Theory for Magnetic Semiconductors with Narrow Bands. *Phys. Status Sol. B* **1974**, *65*, 11. [CrossRef]
20. Nolting, W. Theory of ferromagnetic semiconductors. *Phys. Status Sol. B* **1979**, *96*, 11. [CrossRef]
21. Kochelaev, B.I. Spin-Phonon Interaction and the EPR Linewidth in La_2CuO_4 and Related Cuprates. *J. Supercond.* **1999**, *12*, 53. [CrossRef]
22. Tserkovnikov, Yu.A.; Decoupling of chains of equations for two-time Green's functions. *Teor. Mat. Fiz.* **1971**, *7*, 250. [CrossRef]
23. Apostolova, I.N.; Apostolov, A.T.; Wesselinowa, J.M. Multiferroic and phonon properties of pure and ion doped $CoCr_2O_4$-Bulk and nanoparticles. *J. All. Comp.* **2021**, *852*, 156885. [CrossRef]
24. Katsura, H.; Nagaosa, N.; Balatsky, A.V. Spin current and magnetoelectric effect in noncollinear magnets. *Phys. Rev. Lett.* **2005**, *95*, 057205. [CrossRef] [PubMed]
25. Vaks, V.G. *Introduction to the Microscopic Theory of Ferroelectrics*; Nauka: Moscow, Russia, 1973; p. 158. (In Russian)
26. Goryachev, E.; Kuzmin, E.V.; Ovchinnikov, S.G. Metal-insulator transition in the Hubbard model by the irreducible Green functions method. *J. Phys. C* **1982**, *15*, 1481. [CrossRef]
27. Lawes, G.; Melot, B.; Page, K.; Ederer, C.; Hayward, M.A.; Proffen, T.; Seshadri, R. Dielectric anomalies and spiral magnetic order in $CoCr_2O_4$, *Phys. Rev. B* **2006**, *74*, 024413. [CrossRef]
28. Kocsis, V.; Bordacs, S.; Varjas, D.; Penc, K.; Abouelsayed, A.; Kuntscher, C.A.; Ohgushi, K.K.; Tokura Y.; Kezsmarki, I. Magnetoelasticity in ACr_2O_4 spinel oxides (A = Mn, Fe, Co, Ni, and Cu). *Phys. Rev. B* **203**, *87*, 064416. [CrossRef]
29. Wesselinowa, J.M.; Apostolov, A.T. Anharmonic effects in ferromagnetic semiconductors. *J. Phys. Cond. Matter* **1996**, *8*, 473–488. [CrossRef]
30. Xu, Y.; Liu, X.; Kan, X.; Feng, S.; Wang, W.; Liu, C.; Li, Y. Synthesis and Analysis of Zn-Substituted $CoCr_2O_4$ Spinel Oxide. *J. Supercond. Novel Magn.* **2022**, *35*, 753–762. [CrossRef]
31. Hosseini, S.G.; Abazari, R.; Gavi, A. Pure $CuCr_2O_4$ nanoparticles: Synthesis, characterization and their morphological and size effects on the catalytic thermal decomposition of ammonium perchlorate. *Solid State Sc.* **2014**, *37*, 72–79.
32. Ortuno-Lopez, M.B.; Sotelo-Lerma, M.; Mendoza-Galvana, A.; Ramirez-Bona, R. Optical band gap tuning and study of strain in CdS thin films. *Vacuum* **2004**, *76*, 181. [CrossRef]